Proceedings of the Canadian Society for Mechanical Engineering International Congress
32nd Annual Conference of the Computational Fluid Dynamics Society of Canada
Canadian Society of Rheology Symposium
CSME/CFDSC/CSR 2025
May 25–28, 2025, Montréal, Québec, Canada

Large Eddy Simulations of Freely Evolving and Colliding Human Exhalation Flows

Ryid Gilani[1], Abbas Ghasemi[1,*]

[1]Mechanical, Industrial, and Mechatronics Department, Toronto Metropolitan University, Toronto, Canada
ryid.gilani@torontomu.ca, *a.ghasemi@torontomu.ca

***Abstract*—**Large eddy simulations (LES) are performed to investigate the characteristics of freely evolving and colliding jets, representative of human exhalation, at Reynolds numbers Re = 700 and 1400. The study examines the effects of three mouth shapes with aspect ratios (AR = 1, 2, 4) and two colliding momentum ratios (M = 1, 2). The axial and lateral extent of the flows is quantified and validated against experimental data, with implications for pathogen transport in unshielded conversations. The LES results capture key characteristics of starting and transitioning circular/elliptic jets, providing valuable insight into the formation and evolution of vortical structures carrying the exhaled pathogens. The colliding flow interactions are strongly influenced by whether the collision is symmetric (M = 1) or asymmetric (M = 2). Symmetric collisions lead to lateral flow redirection, forming a stagnation plane or "blocking effect" at the center of the domain, which reduces pathogen transmission. In contrast, asymmetric collisions result in a weaker blocking effect, as the stronger jet overpowers the weaker one leading to an increased risk of exposure for the weaker speaker.

***Keywords-component*—Large eddy simulation (LES); Vortical structures; Human exhalation**

I. INTRODUCTION

Respiratory infections caused by various viruses/pathogens have led to moderate to severe illnesses across a significant portion of the global population, resulting in high mortality rates among individuals with underlying medical conditions such as cardiovascular disease, diabetes, chronic respiratory disease, and cancer. Given the airborne nature of host-to-host transmission [1], [2], it is essential to explore the interaction between fluid flow and pathogen transport [3]. This becomes particularly crucial when infected and susceptible individuals are in close proximity, where their breathing patterns dominate the transmission of pathogen-laden respiratory droplets. The interaction of exhaled air streams with ambient airflow, particularly in poorly ventilated indoor spaces [4], [5], plays a significant role in preventing or facilitating the spread of airborne pathogens. Notably, super-spreading events often occur in such environments [6]–[8]. The present study focuses on understanding the fundamental fluid mechanics of respiratory transmission, with particular attention given to breathing patterns resembling starting or transitioning jets.

Jet flows, with dynamics similar to those of speech-related exhalation, emerge when a shear layer develops due to the instability at the interface between high-velocity and low-velocity fluid regions. This instability, known as the Kelvin-Helmholtz (KH) instability, initially evolves linearly before transitioning into a nonlinear state, forming vortical structures that influence the shear and rotation zones of the flow [9]. When the fluid is expelled through circular openings, axisymmetric shear layers or round jets are generated [10]–[13]. The formation of KH vortex rings [14], [15], alongside viscous diffusion and small/large-scale entrainment, governs the spatiotemporal evolution of round jets [16], [17].

In the context of speech-related airflow, a round jet can represent the airflow pattern produced when pronouncing the letter "O". Pronouncing other sounds, such as "E", reshape the mouth into a non-circular opening (e.g., square, rectangular, elliptical, or diamond-shaped), leading to non-circular jet-like exhalation [18]–[21], with more complex three-dimensional dynamics [22]–[25]. Due to differences in their penetration rates and lateral spreading, non-circular jets interact with ambient air differently than round jets [26], altering mixing characteristics [27]–[30]. This effect is particularly pronounced in the near-field region, where azimuthal perturbations in the asymmetric vortex rings enhance self-induced distortions [31]–[36]. However, farther downstream, non-circular jets often transition into more symmetric shapes [37], [38].

Several experimental and numerical studies have investigated the dynamics of human exhalation in the context of transitioning jet-like flows and puffs [39]–[43]. Others focus on speech signals that contain plosive sounds and quantify their characteristics, describing them as a train of puffs propelling each other further downstream over time [44]. Various studies also introduce particles into their simulations and determine

the probability of inhalation for a susceptible speaker [45]–[47] to provide insights into airborne transmission mechanisms, the influence of mouth shape, flow structures, and ambient interactions on respiratory aerosol dispersion.

In this study, large eddy simulations (LES) are conducted and validated against existing experimental data [45] to better understand the dynamics of starting jet-like breathing patterns. To achieve this, the study simulates the different aspect ratio (AR) freely evolving jet flows for round jets (AR = 1) and elliptical jets (AR = 2, 4). These cases are used to investigate the evolution of breathing flows corresponding to different mouth shapes during exhalation. Additionally, four other simulations are performed to analyze the head-on collision of two exhaled air streams originating from different mouth shapes and momentum ratios. By examining these seven cases, the study aims to provide insights into the velocity and vorticity [48], [49] dynamics of jet-like breathing flows. At this stage, the analysis is focused on a single-phase flow assumption, where airborne pathogens are assumed to faithfully follow the air stream without significantly affecting the fluid motion. Future work will extend this study to multiphase simulations, incorporating respiratory droplets of varying sizes and their interactions with the exhaled airflow.

II. Computational Methodology

Large eddy simulations (LES) are performed in COMSOL Multiphysics 6.2 using the LES Smagorinsky (`spf`) interface [50]. The governing equations consist of the continuity equation for mass conservation (1),

$$\rho \nabla \cdot (\mathbf{u} + \mathbf{u}') = 0 \tag{1}$$

and the filtered Navier-Stokes equation for momentum (2):

$$\rho \frac{\partial(\mathbf{u} + \mathbf{u}')}{\partial t} + \nabla \cdot \Big(\rho \mathbf{u}\mathbf{u}^T + \rho \mathbf{u}\mathbf{u}'^T + \rho \mathbf{u}'\mathbf{u}^T + p'\mathbf{I} \Big) = \nabla \cdot \Big(-p\mathbf{I} + \mathbf{K} \Big) + \mathbf{F} \tag{2}$$

Here, $\mathbf{u}$ and $\mathbf{u}'$, represent the resolved and sub-grid scale components of the velocity field, respectively. Similarly, p and p' represent the resolved and unresolved components of pressure, respectively. The subgrid-scale stress tensor, $\mathbf{K}$, which is responsible for modeling the effects of unresolved turbulence, contains a tuning parameter for the turbulent viscosity called the Smagorinsky parameter, C_s [51]. In this work C_s = 0.1, which is the default value. Due to the nature of the LES, the study is both three-dimensional and time-dependent, employing a second-order (P2+P2) discretization of fluids for both velocity and pressure [52]. The Generalized-Alpha implicit time-stepping scheme with the Algebraic Multigrid (AMG) method is applied as a solver. The equations are spatially discretized using the Finite Element Method (FEM).

A. Computational Domain and Boundary Conditions

The computational domains for the present LES simulations are modeled to resemble the experimental setup of Giri et al [45] for validation purposes. The single jet (free flow) case and the colliding cases, respectively have the dimensions ($L_x \times L_y \times L_z$) of ($0.25\,\text{m} \times 0.096\,\text{m} \times 0.096\,\text{m}$) and ($0.25\,\text{m} \times 0.3\,\text{m} \times 0.3\,\text{m}$). A multi-cone meshing approach shown in Figure 1 is employed to enhance meshing efficiency and capture the flow physics accurately (See more details in Tables I and II). Air is the working fluid, with a dynamic viscosity $\mu = 1.85 \times 10^{-5}$ kg/(m·s), at a temperature 20°C. Transient exhalations are issued into the domain through the circular (aspect ratios AR= 1) inlet representing the mouth with a diameter of 0.0064 m, flushed at (0,0,0), and (0.25,0,0) for the colliding cases. Two other elliptic inlets (with AR=2, 4) are generated with equivalent circular diameter. A top hat velocity profile (3) is assigned to the inlet(s):

$$V(y,z) = \frac{V_{cl}}{2}\left(1 + \tanh\left(\frac{D_{eq}}{\theta}\left(1 - \frac{\left(\frac{y}{a}\right)^2 - \left(\frac{z}{b}\right)^2}{\sqrt{\left(\frac{y}{a}\right)^2 + \left(\frac{z}{b}\right)^2}}\right)\right)\right) \tag{3}$$

Where, $V(y,z)$ represents the jet inlet velocity distribution, and V_{cl} is the jet centerline velocity, calculated as 1.66 m/s. The parameters y and z denote the spatial coordinates perpendicular to the jet axis, while a and b represent the semi-major and semi-minor axes of an elliptic inlet, respectively. For the circular nozzle, these values are equal, $a = b = 0.0032$ m. The equivalent diameter of the inlet is given as $D_{eq} = 2\sqrt{ab} = 0.0064$ m. The momentum thickness $\theta = 0.00064$ is specified as 10% of the equivalent diameter. Synthetic turbulence of 10% is also applied at the inlet(s). The four lateral faces of the domain are assigned as outlets, while no-slip conditions are enforced on both the inlet face and the opposite wall.

TABLE. I: Cone Dimensions in Figure 1a

Cone	Smaller Diameter (m)	Larger Diameter (m)	Length (m)
Smallest	0.0064	0.0128	0.032
2nd Smallest	0.0128	0.0256	0.0768
2nd Largest	0.0192	0.0384	0.16
Largest	0.0256	0.0512	0.25

TABLE. II: Cone Dimensions in Figure 1b

Cone	Smaller Diameter (m)	Larger Diameter (m)	Length (m)
Smallest	0.0064	0.0128	0.032
2nd Smallest	0.0128	0.0256	0.064
2nd Largest	0.0192	0.0384	0.096
Largest	0.0256	0.2	0.125

B. LES mesh specifications

The multi-cone tetrahedral meshing approach ensures accurately resolved flow structures and computational efficiency. The refined elements in critical regions are gradually coarsened following the growth of the vortical structures farther downstream. The mesh independence study in Figure 2 confirms sufficient grid refinement, with a total of 3,788,065 and

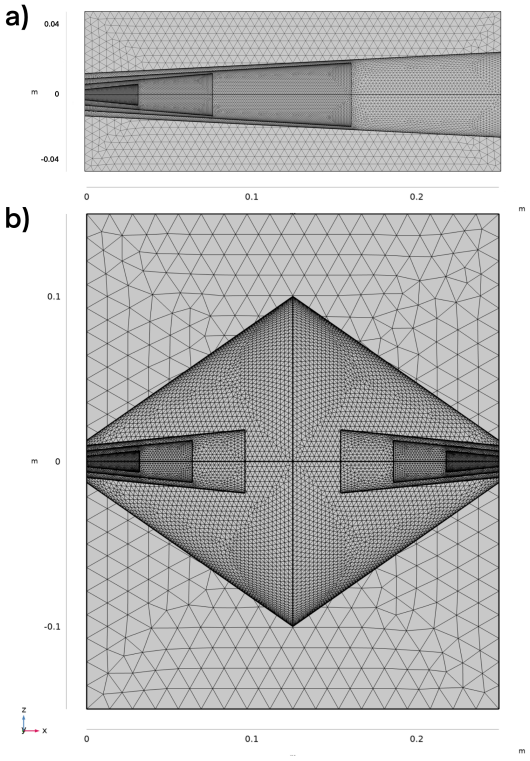

Figure. 1: Computational domain and mesh for (a) free and (b) colliding exhalation

TABLE. III: Mesh Statistics for each cone in Figure 1a

Cone	Minimum Element Size (m)	Maximum Element Size (m)
Smallest	0.000083	0.0005
2nd Smallest	0.0005	0.000884
2nd Largest	0.000884	0.00111
Largest	0.00142	0.002036

2,444,004 mesh elements, respectively, presented in Figures 1a and 1b, with detailed statistics given in Table 3 and Table 4. For computational considerations, the colliding cases are refined within the collision zone, and more high-resolution simulations are ongoing. The minimum grid size to the minimum Kolmogorov length scale ratio ($\frac{\Delta_{min}}{\eta_{min}}$) is estimated to vary from 10.85 to 15.34, which is sufficient to resolve the majority of micro-scales scales contributing to dissipation.

TABLE. IV: Mesh Statistics for each cone in Figure 1b

Cone	Minimum Element Size (m)	Maximum Element Size (m)
Smallest	0.00014525	0.000875
2nd Smallest	0.000875	0.001547
2nd Largest	0.001547	0.002485
Largest	0.002485	0.003563

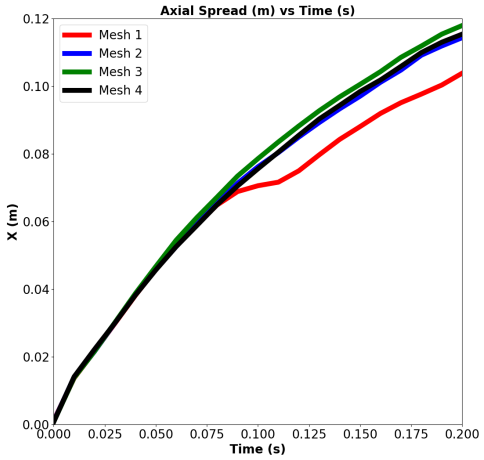

Figure. 2: Mesh Independence

III. RESULTS AND DISCUSSIONS

A. *Validation of the simulations*

Comparing the present LES with the experiments by Giri et al. [45] in Figures 3-5, shows reasonable agreement of axial penetration and lateral width of the free exhalation jet in (ZX) and (XY) planes, while instantaneous lateral contractions and expansions lead to local deviations.

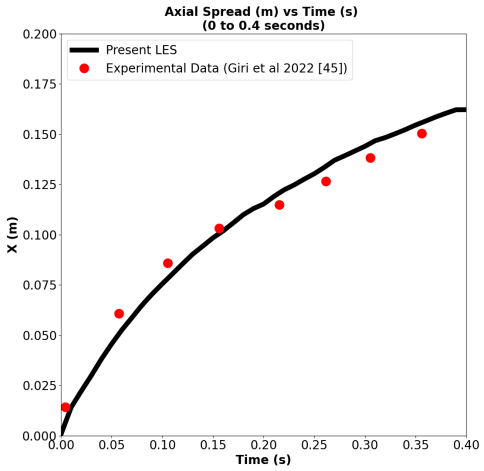

Figure. 3: Axial Penetration of the Free Exhalation: Present LES vs. Experiments from Giri et al [45]

B. *Freely evolving jet-like exhalation*

The free exhalation in Figure 6 penetrates linearly at a constant initial velocity until vortex formation, entrainment, and ambient resistance decelerate the tip, leading to an asymptotic penetration. This transition from momentum-driven motion to vortex-dominated deceleration explains the observed evolution of the simulated free exhalation flows that resemble starting jet flows. It can also be seen that the evolution of the stream flow is affected by the shape of the mouth when the aspect ratio of the opening is varied (AR = 1,2,4). In particular, jet penetration is slower with increased AR, due to self-induced deformations,

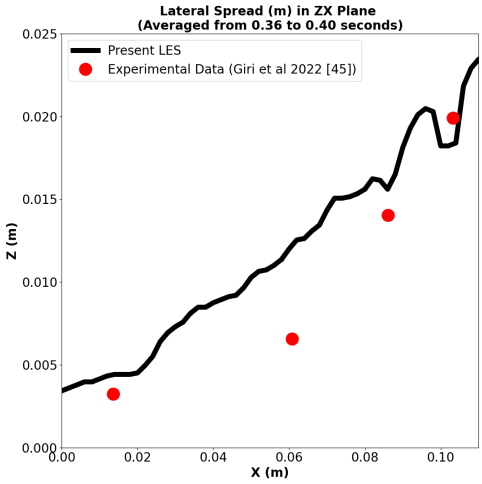

Figure. 4: Lateral (ZX) Width of the Free Exhalation: Present LES vs. Experiments from Giri et al [45]

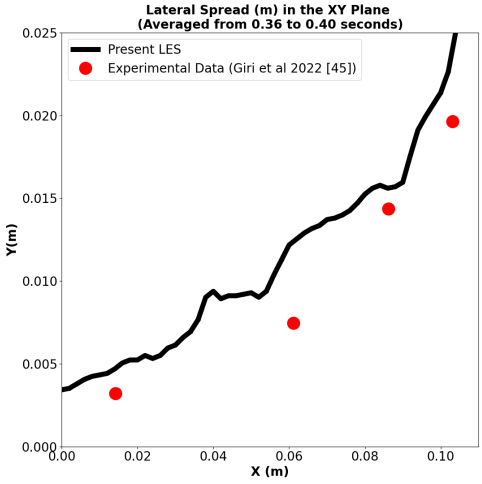

Figure. 5: Lateral (XY) Width of the Free Exhalation: Present LES vs. Experiments from Giri et al [45]

axis-switching, and stronger lateral demonstrated by the lateral width profiles in Figures 7 and 8.

The freely exhaled jet penetrations and the lateral widths are visualized in Figure 9 using the vorticity magnitudes in the (ZX) and (XY) planes, revealing shear layer formation in the near-field regions. A leading vortex ring is formed and followed by the trailing shear layer, which becomes unstable due to the Kelvin-Helmholtz (KH) instability. With downstream distance, the jets evolve laterally due to viscous diffusion small/large-scale entrainment. Unlike the circular case, the non-circular exhalation jets undergo different growth rates in the two orthogonal mid-planes. The axis-switching is initiated by the curvature-induced deformations of the non-circular vortex rings in the near-field and continues until the cross-section becomes rather symmetric farther downstream. The free jet-like breathing from different mouth shapes can affect the streamwise and spanwise spread of the flow and,

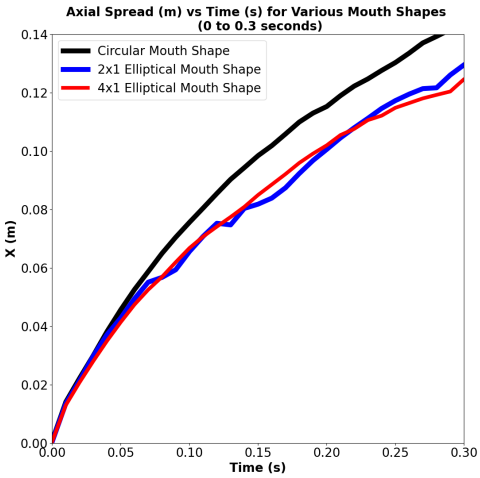

Figure. 6: Axial Spread of Free Exhalation (M=1,2,4)

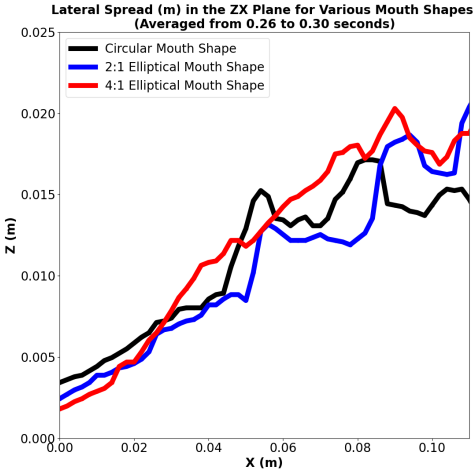

Figure. 7: Lateral Spread (ZX) of Free Exhalation (M=1,2,4)

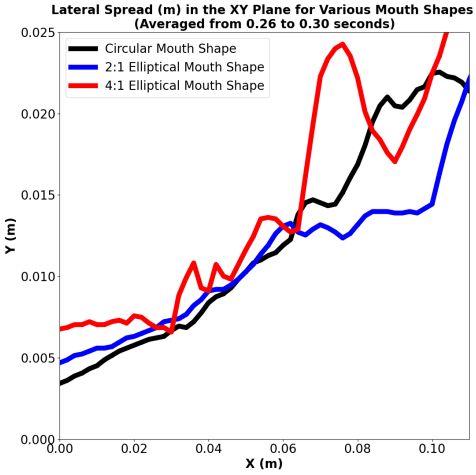

Figure. 8: Lateral Spread (XY) of Free Exhalation (M=1,2,4)

correspondingly, the pathogen transport.

C. Colliding exhalation jets

Figure 10 exhibits the iso-surfaces of vorticity magnitude colored by pressure in colliding exhalation jets. In contrast to the freely evolving breath where only the infectious person breathes/speaks and the susceptible individual exhales negligibly, both speakers generate a jet-like flow for the colliding cases. When both individuals exhale, pathogen transport is governed by symmetric (M = 1) or asymmetric (M = 2) collision of the breathing streams. In a symmetric collision, where exhalation jets have a momentum ratio M=1, impinging jets lead to vortex break-down and lateral flow redirection. As a result, a stagnation zone is formed causing a "blocking effect" in the mid-plane of the domain. This will result in a reduced risk of exposure for the susceptible person. In asymmetric exhalation, the infectious jet has a momentum twice (M=2) that of the susceptible person. Therefore, a weaker blocking effect shifts the stagnation zone closer to the susceptible person leading to increased risk of exposure.

IV. CONCLUSIONS

Fluid physics of freely evolving and colliding exhalation are studied using Large eddy simulations (LES). Freely exhaled jets from the infectious person evolve unboundedly towards the susceptible person breathing/speaking negligibly, hence increasing the risk of exposure. The circular/elliptic mouth shapes of different aspect ratios (AR=1,2,4), alter the streamwise/spanwise spread of the exhaled jets due to self-induced deformations. When both individuals speak, transmission dynamics are significantly affected by the exhaled momentum ratios. In colliding cases, laterally redirected vortical structures create a stagnation region, where a "blocking effect" reduces the exposure to infectious pathogens. These findings suggest that higher infectious-to-susceptible exhalation momentum ratios increase the exposure risk for the weaker speaker.

REFERENCES

[1] L. Bourouiba, "Fluid dynamics of respiratory infectious diseases," *Annual Review of Biomedical Engineering*, vol. 23, pp. 547–577, 2021.

[2] L. Morawska, J. Allen, W. Bahnfleth, P. M. Bluyssen, A. Boerstra, G. Buonanno, J. Cao, S. J. Dancer, A. Floto, F. Franchimon, *et al.*, "A paradigm shift to combat indoor respiratory infection," *Science*, vol. 372, no. 6543, pp. 689–691, 2021.

[3] L. Bourouiba, "The fluid dynamics of disease transmission," *Annual Review of Fluid Mechanics*, vol. 53, pp. 473–508, 2021.

[4] Z. Peng, A. Pineda, E. Kropff, W. Bahnfleth, G. Buonanno, S. Dancer, J. Kurnitski, Y. Li, M. Loomans, L. C. Marr, *et al.*, "Covid-19 indoor airborne transmission risk estimation based on practical risk indicators or co_2 level," in *AGU Fall Meeting 2021*, AGU, 2021.

[5] H. C. Burridge, R. K. Bhagat, M. E. Stettler, P. Kumar, I. De Mel, P. Demis, A. Hart, Y. Johnson-Llambias, M.-F. King, O. Klymenko, *et al.*, "The ventilation of buildings and other mitigating measures for covid-19: a focus on wintertime," *Proceedings of the Royal Society A*, vol. 477, no. 2247, p. 20200855, 2021.

[6] L. Wessendorf, E. Richter, B. Schulte, R. M. Schmithausen, M. Exner, N. Lehmann, M. Coenen, C. Fuhrmann, A. Kellings, A. Huesing, *et al.*, "Analysis of the dynamics, outcome, and prerequisites of the first german sars-cov-2 superspreading event," *medRxiv*, 2021.

[7] M. Z. Bazant and J. W. Bush, "A guideline to limit indoor airborne transmission of covid-19," *Proceedings of the National Academy of Sciences*, vol. 118, no. 17, 2021.

[8] M. Z. Bazant, O. Kodio, A. E. Cohen, K. Khan, Z. Gu, and J. W. Bush, "Monitoring carbon dioxide to quantify the risk of indoor airborne transmission of covid-19," *medRxiv*, 2021.

[9] A. Ghasemi, B. A. Tuna, and X. Li, "Shear/rotation competition during the roll-up of acoustically excited shear layers," *Journal of Fluid Mechanics*, vol. 844, pp. 831–854, 2018.

[10] C. Bogey and C. Bailly, "Large eddy simulations of transitional round jets: influence of the reynolds number on flow development and energy dissipation," *Physics of Fluids*, vol. 18, no. 6, p. 065101, 2006.

[11] A. Ghasemi, A. Pereira, and X. Li, "Large eddy simulation of compressible subsonic turbulent jet starting from a smooth contraction nozzle," *Flow, Turbulence and Combustion*, vol. 98, no. 1, pp. 83–108, 2017.

[12] T. Matsuda and J. Sakakibara, "On the vortical structure in a round jet," *Physics of Fluids*, vol. 17, no. 2, p. 025106, 2005.

[13] T. B. Gohil, A. K. Saha, and K. Muralidhar, "Direct numerical simulation of free and forced square jets," *Flow, Turbulence and Combustion*, vol. 52, pp. 169–184, 2015.

[14] A. K. M. F. Hussain and K. B. M. Q. Zaman, "The preferred mode of the axisymmetric jet," *Journal of Fluid Mechanics*, vol. 110, pp. 39–71, 1981.

[15] S. C. J. Crow and F. H. Champagne, "Orderly structure in jet turbulence," *Journal of Fluid Mechanics*, vol. 48, no. 3, pp. 547–591, 1971.

[16] R. A. Petersen and M. M. Samet, "On the preferred mode of jet instability," *Journal of Fluid Mechanics*, vol. 194, pp. 153–173, 1988.

[17] J. Kim and H. Choi, "Large eddy simulation of a circular jet: effect of inflow conditions on the near field," *Journal of Fluid Mechanics*, vol. 620, pp. 383–411, 2009.

[18] J. Mi and G. J. Nathan, "Statistical properties of turbulent free jets issuing from nine differently-shaped nozzles," *Flow, Turbulence and Combustion*, vol. 84, no. 4, pp. 583–606, 2010.

[19] J. J. Ai, S. C. M. Yu, A. W. K. Law, and L. P. Chua, "Vortex dynamics in starting square water jets," *Physics of Fluids*, vol. 17, no. 1, p. 014106, 2005.

[20] A. Ghasemi, V. Roussinova, and R. Balachandar, "A study in the developing region of square jet," *Journal of Turbulence*, vol. 14, no. 3, pp. 1–24, 2013.

[21] A. Ghasemi, V. Roussinova, R. Balachandar, and R. R. Barron, "Reynolds number effects in the near-field of a turbulent square jet," *Experimental Thermal and Fluid Science*, vol. 61, pp. 249–258, 2015.

[22] E. J. Gutmark and F. F. Grinstein, "Flow control with noncircular jets," *Annual Review of Fluid Mechanics*, vol. 31, no. 1, pp. 239–272, 1999.

[23] F. F. Grinstein, E. Gutmark, and T. Parr, "Near field dynamics of subsonic free square jets. a computational and experimental study," *Physics of Fluids*, vol. 7, no. 6, pp. 1483–1497, 1995.

[24] A. Towne, A. V. G. Cavalieri, P. Jordan, T. Colonius, O. Schmidt, V. Jaunet, and G. A. Brès, "Acoustic resonance in the potential core of subsonic jets," *Journal of Fluid Mechanics*, vol. 825, pp. 1113–1152, 2017.

[25] A. P. Vouros, T. Panidis, A. Pollard, and R. R. Schwab, "Near field vorticity distributions from a sharp-edged rectangular jet," *International Journal of Heat and Fluid Flow*, vol. 51, pp. 383–394, 2015.

[26] Y. Tsuchiya and C. Horikoshi, "On the spread of rectangular jets," *Experiments in Fluids*, vol. 4, no. 4, pp. 197–204, 1986.

[27] W. R. Quinn and J. Militzer, "Experimental and numerical study of a turbulent free square jet," *Physics of Fluids*, vol. 31, no. 5, pp. 1017–1025, 1988.

[28] A. Krothapalli, D. Baganoff, and K. Karamcheti, "On the mixing of a rectangular jet," *Journal of Fluid Mechanics*, vol. 107, pp. 201–220, 1981.

[29] A. Hashiehbaf and G. P. Romano, "Particle image velocimetry investigation on mixing enhancement of non-circular sharp edge nozzles," *International Journal of Heat and Fluid Flow*, vol. 44, pp. 208–221, 2013.

[30] A. J. Yule, "Large scale structure in the mixing layer of a round jet," *Journal of Fluid Mechanics*, vol. 89, no. 3, pp. 413–432, 1978.

[31] C. K. W. Tam and A. T. Thies, "Instability of rectangular jets," *Journal of Fluid Mechanics*, vol. 248, pp. 425–448, 1993.

[32] D. Margerit and J. P. Brancher, "Asymptotic expansions of the biot-savart law for a slender vortex with core variation," *Journal of Engineering Mathematics*, vol. 40, no. 3, pp. 297–313, 2001.

[33] A. Ghasemi, V. Roussinova, R. M. Barron, and R. Balachandar, "Large eddy simulation of the near-field vortex dynamics in starting square jet transitioning into steady state," *Physics of Fluids*, vol. 28, no. 8, p. 085104, 2016.

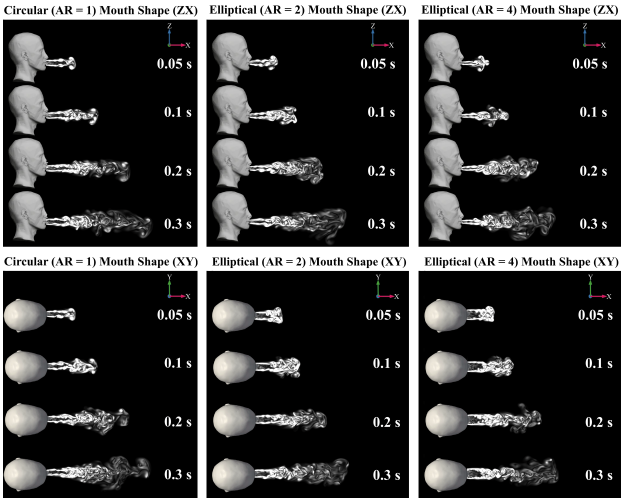

Figure. 9: Evolution of Free Exhalation from Various Mouth Shapes over Time(s)

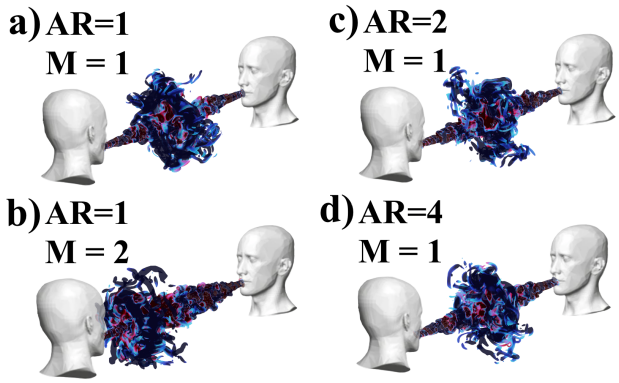

Figure. 10: Isosurface (Level 50) of Vorticity Magnitude (1/s) Coloured with Pressure (Pa) for Various Colliding Breath Cases

[34] A. Ghasemi, B. A. Tuna, and X. Li, "Curvature-induced deformations of the vortex rings generated at the exit of a rectangular duct," *Journal of Fluid Mechanics*, vol. 864, pp. 141–180, 2019.

[35] F. F. Grinstein and C. R. DeVore, "Dynamics of coherent structures and transition to turbulence in free square jets," *Physics of Fluids*, vol. 8, no. 5, pp. 1237–1251, 1996.

[36] F. F. Grinstein, "Vortex dynamics and entrainment in rectangular free jets," *Journal of Fluid Mechanics*, vol. 437, pp. 69–101, 2001.

[37] A. Bejan, S. Ziaei, and S. Lorente, "Evolution: Why all plumes and jets evolve to round cross sections," *Scientific Reports*, vol. 4, p. 4730, 2014.

[38] C.-M. Ho and E. Gutmark, "Vortex induction and mass entrainment in a small-aspect-ratio elliptic jet," *Journal of Fluid Mechanics*, vol. 179, pp. 383–405, 1987.

[39] V. Arumuru, J. Pasa, and S. S. Samantaray, "Experimental visualization of sneezing and efficacy of face masks and shields," *Physics of Fluids*, vol. 32, no. 11, 2020.

[40] J. W. Tang, A. D. Nicolle, C. A. Klettner, J. Pantelic, L. Wang, A. B. Suhaimi, A. Y. L. Tan, G. W. X. Ong, R. Su, C. Sekhar, *et al.*, "Airflow dynamics of human jets: sneezing and breathing potential sources of infectious aerosols," *PLoS One*, vol. 8, no. 4, p. e59970, 2013.

[41] M. El Hassan, H. Assoum, N. Bukharin, H. Al Otaibi, M. Mofijur, and A. Sakout, "A review on the transmission of covid-19 based on cough/sneeze/breath flows," *The European Physical Journal Plus*, vol. 137, no. 1, p. 1, 2022.

[42] C. Xu, P. V. Nielsen, L. Liu, R. L. Jensen, and G. Gong, "Human exhalation characterization with the aid of schlieren imaging technique," *Building and Environment*, vol. 112, pp. 190–199, 2017.

[43] H. Salati, D. F. Fletcher, M. Khamooshi, J. Dong, K. Ito, S. Vahaji, and K. Inthavong, "Exhaled jet and viral-laden aerosol transport from nasal sneezing," *Aerosol and Air Quality Research*, vol. 22, no. 4, p. 210338, 2022.

[44] M. Abkarian, S. Mendez, N. Xue, F. Yang, and H. A. Stone, "Speech can produce jet-like transport relevant to asymptomatic spreading of virus," *Proceedings of the National Academy of Sciences of the United States of America*, vol. 117, no. 41, pp. 25237–25245, 2020.

[45] A. Giri, N. Biswas, D. L. Chase, N. Xue, M. Abkarian, S. Mendez, S. Saha, and H. A. Stone, "Colliding respiratory jets as a mechanism of air exchange and pathogen transport during conversations," *Journal of Fluid Mechanics*, vol. 930, p. R1, 2022.

[46] S. Balachandar, S. Zaleski, A. Soldati, G. Ahmadi, and L. Bourouiba, "Host-to-host airborne transmission as a multiphase flow problem for science-based social distance guidelines," *International Journal of Multiphase Flow*, vol. 132, p. 103439, 2020.

[47] R. Singhal, S. Ravichandran, R. Govindarajan, and S. S. Diwan, "Virus transmission by aerosol transport during short conversations," *Flow*, vol. 2, p. E13, 2022.

[48] B. Van Leer, "On the identification of a vortex," *Journal of Fluid Mechanics*, vol. 285, pp. 69–94, 1995.

[49] S. B. Pope, *Turbulent Flows*. Cambridge University Press, 2000.

[50] COMSOL Multiphysics, *The LES Smagorinsky Interface*, 2022.

[51] COMSOL Multiphysics, *CFD Module User's Guide*, 2020.

[52] P. M. Gresho and R. L. Sani, *Incompressible Flow and the Finite Element Method, Volume 2: Isothermal Laminar Flow*. John Wiley and Sons, Inc., 1998.